HHS Public Access

Author manuscript

J Mol Cell Cardiol. Author manuscript; available in PMC 2018 July 01.

Published in final edited form as:

J Mol Cell Cardiol. 2017 July ; 108: 127–137. doi:10.1016/j.yjmcc.2017.06.001.

The Structural Basis of Alpha-Tropomyosin Linked (Asp230Asn) Familial Dilated Cardiomyopathy

ML Lynn[1,*], **L Tal Grinspan**[2,*,1], **TA Holeman**[1,3], **J Jimenez**[4], **J Strom**[5], and **JC Tardiff**[1,5,6]

[1]Department of Physiological Sciences University of Arizona, Tucson, Arizona 85724

[2]Department of Medicine, Columbia University, New York, New York 10032

[3]Department of Chemistry University of Arizona, Tucson, Arizona 85721

[4]Department of Medicine, Washington University in Saint Louis, St. Louis, MO 63130

[5]Department of Cellular and Molecular Medicine University of Arizona, Tucson, Arizona 85724

[6]Department of Medicine University of Arizona, Tucson, Arizona 85724

Abstract

Recently, linkage analysis of two large unrelated multigenerational families identified a novel dilated cardiomyopathy (DCM)-linked mutation in the gene coding for alpha-tropomyosin (*TPM1*) resulting in the substitution of an aspartic acid for an asparagine (at residue 230). To determine how a single amino acid mutation in α-tropomyosin (Tm) can lead to a highly penetrant DCM we generated a novel transgenic mouse model carrying the D230N mutation. The resultant mouse model strongly phenocopied the early onset of cardiomyopathic remodeling observed in patients as significant systolic dysfunction was observed by 2 months of age. To determine the precise cellular mechanism(s) leading to the observed cardiac pathology we examined the effect of the mutation on Ca^{2+} handling in isolated myocytes and myofilament activation *in vitro*. D230N-Tm filaments exhibited a reduced Ca^{2+} sensitivity of sliding velocity. This decrease in sensitivity was coupled to increase in the peak amplitude of Ca^{2+} transients. While significant, and consistent with other DCMs, these measurements are comprised of complex inputs and did not provide sufficient experimental resolution. We then assessed the primary structural effects of D230N-Tm. Measurements of the thermal unfolding of D230N-Tm vs WT-Tm revealed an increase in stability primarily affecting the C-terminus of the Tm coiled-coil. We conclude that the D230N-Tm mutation induces a decrease in flexibility of the C-terminus via propagation through the helical structure of the protein, thus decreasing the flexibility of the Tm overlap and impairing its ability to regulate contraction. Understanding this unique structural mechanism could provide novel targets for eventual therapeutic interventions in patients with Tm-linked cardiomyopathies.

Corresponding Author: Jil C. Tardiff, Department of Medicine and Cellular and Molecular Medicine, The University of Arizona, Tucson, AZ 85724. (520-626-8001), jtardiff@email.arizona.edu.

*These authors contributed equally to this work

Disclosures

None

Keywords

Cardiomyopathy; Dilated; Mutation; Tropomyosin; Mice; Transgenic

Introduction

While the genetic basis of hypertrophic and dilated cardiomyopathy (HCM, DCM) is widely recognized, our understanding of the precise mechanisms whereby mutations lead to complex cardiac pathology is incomplete [1]. By the time many patients present with symptoms, pathologic cardiac remodeling has progressed past the initial stages and therapeutic options are limited to symptom palliation [2]. Therefore, to establish meaningful genotype-phenotype relationships, it is important to develop animal models that phenocopy the human disorder as a tool to study progressive disease pathophysiology across multiple levels of biological complexity.

A pathogenic mutation was identified in Tm, Asp230Asn (D230N), in two large unrelated multigenerational families and linked to a severe, often early onset DCM [3]. The substitution of an Asn from an Asp at residue 230 results in a charge loss at a solvent exposed residue (f-position) proximal to the C-terminus of Tm (Figure 1) [4]. Affected family members exhibited reduced ejection fraction and enlargement of the left ventricle with a high degree of penetrance (80%). *In vitro* ATPase studies of the D230N mutation in reconstituted cardiac thin filaments demonstrated decreases in maximum ATPase activity, Ca^{2+} sensitivity, Ca^{2+} affinity and cooperativity of Ca^{2+} binding compared to WT-Tm filaments consistent with previous data in other models of DCM [3, 5].

The cardiac thin filament is responsible for the regulation of contraction and relaxation of the sarcomere, the fundamental contractile unit of cardiac muscle. The functional unit of the regulatory thin filament comprises seven actin monomers, one α-tropomyosin (Tm) dimer, and one troponin (Tn) complex. The actomyosin “gatekeeper” Tm plays a critical role in regulating cross bridge formation [6, 7]. Its azimuthal position on actin is in equilibrium between three states (blocked, closed, and open) that determine myosin’s ability to bind to actin and is partially regulated by intracellular Ca^{2+} concentrations [8]. During diastole, Ca^{2+} levels in the cytoplasm are low and the “blocked” position of Tm inhibits the interaction of actin and myosin. At the onset of systole, intracellular Ca^{2+} rises and via a series of allosteric interactions with the other components of the thin filament, Tm is shifted to its “closed” position, partially revealing myosin binding sites on actin, resulting in the formation of weakly bound cross bridges. As more of these weak interactions between actin and myosin form, Tm shifts to its “open” state and strong force-generating cross bridges are formed. In addition, each α-helical coiled coil Tm dimer interdigitates with the adjacent dimer in a head to tail (C to N terminal) array forming a continuous, flexible filament that strengthens its interaction with actin (Figure 1) [4, 6]. This interaction is further stabilized by an alpha helical component of the cTnT N-terminal domain, allowing for the flexibility and stability required to support the dynamic range of motion along actin necessary for the regulation of cross bridge cycling [9]. The flexibility conferred on Tm via cTnT and its many weak electrostatic interactions with actin are central to its regulatory role as it must be

able to rotate substantially around actin to maintain its position in the actin groove [10, 11]. Given the specificity of these complex interactions, it is not surprising that a single amino acid substitution in Tm could have a profound impact on its association with actin and cTnT and therefore its ability to regulate contraction leading to pathology [12]. Moreover, as we and others have previously shown, mutations in thin filament proteins can cause allosteric effects that alter the structure of a protein at sites “at a distance” from the actual mutations in cTnT and Tm [13–15].

In this study our goal was to establish a heterozygous transgenic murine model of Tm D230N - linked DCM with a strong progressive phenotype to first facilitate an interrogation of the whole heart and cellular impact of the mutation. We then coupled these measurements to structural studies to provide an integrative measurement of disease pathogenesis at multiple levels of biological complexity. We hypothesize that the D230N mutation alters Tm flexibility via propagation to the critical Tm overlap region (Figure 1) thus altering thin filament regulatory function. Our results indicate that the flexibility of Tm, central to the regulatory function of the thin filament, is compromised in the presence of the D230N mutation and likely leads to the observed pathology. Furthermore, these data suggest an intrinsic link between the flexibility of Tm and altered whole heart function in a mouse model of human dilated cardiomyopathy.

Materials and Methods

D230N-Tm Transgenic Mouse Model Development

D230N constructs were generated as previously described [16]. Full-length Tm was cloned into a universal cardiac transgenic vector (UCTV) that includes a rat alpha-myosin heavy chain (MHC) promoter and a mouse β^{maj} globin gene terminator (gDEF) [17]. Primers used in the development of the D230N-Tm construct are listed in Table S1. The transgenic constructs were digested with KpnI and SacII yielding a 6 kb fragment that was introduced into FVB mice via pronuclear injection as previously described and backcrossed for >10 generations to C57Bl/6 mice [16]. Transgenic mice were identified by PCR using α-MHC forward and Tm reverse primers (Table S2).

Myofibrillar Protein Preparation

Total myofibrillar protein was prepared as previously described with slight modification [16]. Briefly, hearts were excised and ventricles were dissected in relax buffer [standard rigor buffer (SRB: 75 mM KCl, 10 mM imidazole, 2 mM $MgCl_2$, 2 mM EGTA, 1 mM sodium azide, 1 mM DTT, 5μg/ml Leupeptin, 1μg/ml Pepstatin, 0.1 mM PMSF, 1 mM Benzamidine-HCl) + 4mM Creatine Phosphate, 1 mM ATP. 50mM BDM, 1% Triton X-100]. Ventricles were homogenized in rapid rigor buffer (SRB + 25 mM EDTA) and myofibrils were collected by centrifugation. Myofibrils were then washed in SRB + 1% Triton X-100. The spin/wash steps were repeated with SRB + 1% Triton X-100, then twice with SRB. Finally, myofibrils were re-suspended in SRB. Protein concentration was quantified using Pierce BCA™ Protein Assay Kit with bovine serum albumin as a standard.

One-Dimensional Isoelectric Focusing (ID-IEF) for Transgene Expression

ID-IEF using slab gel electrophoresis was performed on 10 μg of total myofibrillar protein as previously described with modification [18]. Briefly, IEF gel slabs (0.75 mm thick) containing 5% acrylamide/bis (37.5:1, Biorad, Hercules, CA), 9.1 M urea, 2% (w/v) Triton X-100, and 0.05× of Pharmalyte 4.2–4.9 (GE Healthcare, Chicago, IL), with the catalysts ammonium persulfate and N,N,N,N-tetramethylethylenediamine (TEMED) added separately. Myofibrillar protein samples were prepared in IEF solubilization buffer containing 9.2 M urea (Biorad, Hercules, CA), 2% Triton X-100, 0.02× of Pharmalyte 4.2–4.9, Tributyl Phosphine (Biorad, Hercules, CA) and 0.01% Bromophenol Blue (w/v). Electrophoresis was performed using 40 mM lysine as the cathode buffer and 7 mM phosphoric acid as the anode buffer. The gel was transferred in 0.7% acetic acid (pH 3) in preparation for western blotting.

Quantitative Western Blot

Quantitative immunoblotting of cardiac myofibrils was carried out as previously described [19]. Western blot analysis was conducted using a striated muscle Tm specific CH1 antibody followed by peroxidase-labeled goat anti-mouse secondary antibody (Millipore, Billerica, MA). Immunoreactivity was visualized with ECL™ Western Blotting Detection Reagents (GE Healthcare, Chicago, IL) and exposure to x-ray film (CL-X Posure™ Film, Thermo Scientific Waltham, MA). The intensity of the bands was quantified using NIH ImageJ analysis software [20].

Morphology and Histology

Hearts from mutant and Non-Tg mice were rapidly excised and rinsed in PBS. Aorta and pulmonary vessels were dissected off and hearts were fixed in 10% formalin overnight. Sagittal and transverse sections were made to expose ventricular morphology. Hematoxylin and Eosin staining and Masson's Trichrome of paraffin embedded sections was performed as previously described [21].

Echocardiography

Echocardiograms were acquired using the Vevo 770 High-Resolution *In Vivo* Imaging System (Visual Sonics, Toronto, Ontario, Canada). Mice under continuous anesthesia of 1.5% isoflurane were taped onto a platform with Signagel (Parker Laboratories, Fairfield, NJ) to simultaneously acquire electrocardiograms. Parasternal long-axis view at the papillary muscle level and M-mode images were recorded. Echocardiograms were analyzed by tracking left ventricular dimensions through one full cardiac cycle in B-mode acquisition. M-mode acquisition was analyzed by measuring interventricular septum, left ventricle, and posterior wall dimensions during systole and diastole.

Pressure-Volume Loops In vivo

pressure-volume analysis was performed in age matched (3 months) mice as previously described with slight modification [22]. In brief, mice were anesthetized and ventilated with 1.5% isoflurane using a SAR-1000 Small Animal Ventilator (CWE Inc, Ardmore, PA). Body temperature under anesthesia was maintained at 37°C and a lateral incision was made in

order to expose the apex of the heart. A 1.2F catheter was then inserted into the LV. Baseline functional parameters were assessed during a pause in ventilation in order to avoid respiratory artifacts. To obtain load-independent indices, including the end-systolic and end-diastolic pressure-volume relationships, the IVC was temporarily occluded to vary the preload conditions. Data acquisition and analysis was performed using LabScribe 2 (iWorx, Dover, NH) and curve fitting was performed with MATLAB (MathWorks, Natick, MA).

Myocellular Mechanics and Intracellular Ca^{2+} Transients

Ventricular myocytes were dissociated from a minimum of four 4–6-month old mice using a modified protocol as described previously [19, 23]. Cells were kept in 1.2 mM Ca^{2+} loading solution (135 mM NaCl, 4 mM KCl, 10 mM HEPES, 10 mM Glucose, 0.33 mM Na_2HPO_4, 5 mg/ml BSA, 1 mM $MgCl_2$, pH 7.4 + 0.5 mM Probenecid) until they were loaded onto a flow chamber for contractility measurements. Sarcomere length and intracellular Ca^{2+} transients were measured as previously described with modifications [19, 23] using the IonOptix System (IonOptix, Inc., Milton, MA). Cells in loading solution were added to flow chamber and allowed to settle. Adherent myocytes were electrically paced at 1 Hz and field stimulated at 10 V with the Myopacer Cell Stimulator (IonOptix Inc., Milton, MA) while being continuously perfused at 25°C with 1.2 mM Ca^{2+} Tyrode Solution containing 137 mM NaCl, 5.4 mM KCl, 10 mM HEPES, 10 mM Glucose, 0.5 mM Probenecid, 1.2 mM $CaCl_2$ and 1 mM $MgCl_2$, pH 7.4. To test response to β-agonist stimulation experiments 1 μM isoproterenol was added to Tyrode Solution. Cells were viewed using a Nikon Diaphot 200 Inverted Microscope connected to an IonOptix Myocam digital CCD video camera. Sarcomeric edge detection algorithms were used to measure contraction kinetics of cells (SarLen Acquisition System and Ion Wizard version 4.4 Acquisition Software, IonOptix, Inc Milton, MA). Myocellular measurements of contractile function and relaxation were obtained from a minimum of ten transients per cell. Ca^{2+} transients were measured in a separate aliquot of cells loaded with 1 μM Fura-2 AM for 15 minutes and washed with loading solution. Loading solution and Tyrode solution contained 500 mM probenecid to prevent leakage of Fura-2 from cells. Fura-2 loaded myocytes were alternately excited at 340 and 380 nm. Fluorescence emission was collected by a 40× Olympus UApo/340 oil immersion objective and reflected through a barrier filter (510/40 nm) to a photomultiplier tube (IonOptix Inc. Milton, MA). Ca^{2+} transients reported as Fura-2 ratios were generated from the measurements of emission as a function of excitation wavelength with background fluorescence subtracted. Ca^{2+} transient measurements were obtained from a minimum of ten transients per cell.

Tm Expression and Purification

Alanine-serine tagged α-tropomyosin (as-Tm) cDNA in a pET-SUMO vector (a kind gift of Dr. David Wieczorek at the University of Cincinnati) was cloned into the pET3D vector (Millipore, Billerica, MA) and mutated via Quick-Change site-directed mutagenesis (Stratagene, San Diego, CA) to introduce the D230N substitution. The ala-ser tag on Tm mimics the N-terminal acetylation necessary for *in vitro* head-to-tail polymerization, binding to actin and Tn, and regulatory function of the myosin ATPase [24, 25]. WT and D230N mutated as-Tm were transformed into BL21 competent cells (Millipore, Billerica, MA). as-Tm was isolated through a set of pH changes: first lowered to 4.6 with 1 N HCl, centrifuged

at 14,000 rpm for 20 min at 4°C, the pellet was re-suspended with 1 M KCl pH 7.0+and pH was raised above 7.0 with 1 M KOH. The sample was centrifuged again and the acid/base pH changes were repeated three times. The final supernatant was cut with 65% ammonium sulfate, pH was adjusted between 7 and 8, and the solution was centrifuged at 10,000 rpm for 20 minutes at 4°C. These steps were then repeated with 70% ammonium sulfate. The pellet containing Tm was re-suspended in 7.5 mM β-mercaptoethanol (βME) pH > 7.0, then dialyzed at 4°C against 2mM βME pH 7–8 to remove ammonium sulfate.

Troponin Expression and Purification and Reconstitution

The cDNA for human cardiac Troponin I (hcTnI) in a pET11d expression vector (Millipore, Billerica, MA) and human cardiac Troponin C (hcTnC) and Troponin T (hcTnT) in pET3d vectors were provided by Dr. J. D. Potter (University of Miami Medical School). Troponin proteins were expressed, purified, and reconstituted as previously described [26, 27]. The cTn complex was separated from the monomeric troponins by anion exchange on a RESOURCE-Q column (GE Healthcare, Chicago, IL) connected to an AKTA FPLC system (GE Healthcare, Chicago, IL).

Myosin Preparation

Myosin was extracted and prepared from rabbit skeletal muscle as previously described [28]. The myosin solution concentration was determined by absorbance at 280 nm using an extinction coefficient of $0.52 g/L^{-1}cm^{-1}$. A 50:50 myosin:glycerol solution was stored at −20°C. Heavy Meromyosin (HMM) was prepared from glycerinated myosin as previously described [29].

Actin Re-suspension and Labeling

Actin was purified and prepared as previously described [4]. Rhodamine Phalloidin was added to F-Actin at a final concentration of 2 μM, incubated for 1 hour on ice and protected from light.

Regulated In Vitro Motility In vitro

motility assays were performed as previously described [30–33]. Motility was viewed using an Olympus IX-71 (Center Valley, PA) inverted microscope under fluorescence illumination and a 100x objective. Thin filament movement was recorded using a Hamamatsu ORCA-ER cooled CCD (Hamamatsu City, Japan). For each preparation 8–12 sites on a surface were recorded for a minimum of 25 seconds. Using the MetaMorph 7 system (Molecular Devices, Sunnyvale, CA), the movement of each filament in the field of view was recorded using frame-grabbing rates of 5–10 frames/sec. The Track Points program in MetaMorph software was used to track filament centroids and compute their frame-to-frame movements. Mean speeds for at least 100 individual filaments were calculated for each condition. Filaments were classified according to whether they were moving or not, and whether they demonstrate erratic or uniform movements as previously described [30]. Briefly, the motile filaments are divided into two categories: uniformly motile filaments, defined as those with a frame to frame standard deviation < 50% of their mean speed, and erratically motile

filaments, defined as those with frame to frame standard deviation > 50% of their mean speed.

Circular Dichroism

Far-UV circular dichroism (CD) spectra of WT and D230N-Tm were obtained using an Olis DSM-20 (Analytical Biophysics Core, University of Arizona) scanning from 200–260 nm at 20°C. Additionally, the temperature dependence of mean residual elipticity at 222 nm was monitored from 10°C to 70°C at a heating rate of $2°C \cdot min^{-1}$ with a 2-minute equilibration period. Far-UV CD spectra were reported at every temperature as an average of ten scans. The samples contained ~0.3 mg/ml of WT or D230N as-Tm in 50 mM sodium phosphate, pH 7.0, 100 mM NaCl, 1 mM $MgCl_2$, and 1 mM βME. Spectra were confirmed through second heating after samples were cooled back down to 10°C suggesting the presence of thermodynamic equilibrium. Mean residual elipticity was plotted as a function of temperature and the curves were fit in GraphPad (La Jolla, CA) via a non-linear least squares fit and EC50 was calculated [34].

Differential Scanning Calorimetry

WT and D230N Tm were dialyzed in a degassed buffer containing 20 mM MOPS, 0.1 M NaCl, 1 mM EDTA, and 1 mM β-ME, pH 7.0 [12]. The concentrations of samples were: WT-Tm 1.81 mg/mL and D230N-Tm 1.86 mg/mL. Samples were degassed for 5–10 minutes at 10°C prior to loading into the instrument. A NanoDSC (TA Instruments, New Castle, DE) was used to assay the thermal stability of the proteins. For each test, equivalent volumes of buffer and sample were loaded. The instrument scanned from 20 to 70 °C at 1.0 °C/min with a 600 second equilibration. A buffer-buffer scan was also performed and applied as the background. Reversibility was checked by scanning each sample twice, during initial and second heating. All the data was evaluated with the NanoAnalyze Software (TA Instruments, New Castle, DE) package. Due to reversibility of the transitions, the data was fitted with a Van't Hoff two-state model.

Statistical Analysis

All values are reported as mean ± S.E.M. calculated using GraphPad Prism 5 and Prism 7(San Diego, CA). For HW/BW measurements one-way ANOVA with a Newman Keuls post hoc analysis was used for comparison to Non-Tg. Functional parameters (including echocardiographs and PV loops) were analyzed using a student's t-test to compare to Non-Tg. Myocellular mechanics and intracellular calcium transients were analyzed via two-way ANOVA with a Bonferroni post-test. For R-IVM a student's t-test was used for statistical comparison to WT filaments. The thermal stability and structure assessed via DSC and CD was analyzed using an extra sum of squares F-test, least squares fit, and one-way ANOVA for comparison to WT-Tm. For all analyses a p-value of less than 0.05 was accepted as statistically significant.

Results

Generation of Transgenic Lines

To study the pathological effects of the D230N-Tm mutant *in vivo*, Tm carrying the D230N mutation was expressed in mice under the cardiac specific alpha-MHC promoter (Table S1 and S2). Using one-dimensional isoelectric focusing to separate WT and D230N-Tm, high expresser (57%) and low expresser (10%) lines of the D230N transgene were identified (Figure S1). Additionally, mass spectrometry was used to confirm expression levels in the high expressing line and revealed ~69% of the D230N transgene (data not shown). The high and low expressing lines exhibited comparable phenotypes therefore further experiments were carried out with the high expresser, herein referred to as D230N unless otherwise indicated.

Morphological and Histological Characterization of D230N Tm Hearts

Sagittal and transverse sectioning of mouse hearts at 6 months of age revealed dilation of the left ventricles of D230N-high and low expressing transgenic mice (Figure 2). The extent of cardiac enlargement was quantified by measurement of heart weight relative to body weight (HW/BW) at 2 and 6 months. HW/BW measurements revealed that cardiac remodeling was detectable as early as two months in both D230N-high and low hearts compared to Non-Tg siblings. At 6 months both mutant lines exhibited significantly increased HW/BW, but were not significantly different from each other (Figure 2).

Hematoxylin and eosin staining of hearts from D230N-high mice at 6 months of age were negative for inflammatory infiltration (Figure 3A–C) [35, 36]. The only histologic abnormality in these hearts were broadened intercalated discs, a common, non-specific, finding in DCM [37]. Additionally, trichrome stained sections were negative for myocardial fibrosis (Figure 3D–F).

Effect of the D230N Mutation on Cardiac Function

The cardiac function of adult D230N male and female transgenic mice and their Non-Tg siblings was evaluated via echocardiography to follow disease progression and assess the extent of ventricular remodeling (Table 1). At 6 months D230N mice exhibited increased left ventricular chamber size compared to Non-Tg. Diastolic and systolic left ventricular internal diameters ($LVID_{d/s}$) were significantly increased in the D230N mice (4.382 ± 0.081 and 3.356 ± 0.174 mm) compared to Non-Tg (3.844 ± 0.886 and 2.510 ± 0.110 mm). Similarly, end diastolic volume (EDV) and end systolic volume (ESV) of D230N mice (87.01 ± 3.89 and 46.78 ± 6.02 μl) were significantly increased compared to Non-Tg (64.73 ± 4.37 and 23.49 ± 2.95 μl). Cardiac function parameters demonstrated decreased contractile function in the D230N mice compared to Non-Tg siblings. The ejection fraction (%EF) of D230N mice (46.78 ± 4.42 %) was decreased compared to Non-Tg (67.11 ± 3.68 %). Percent fractional shortening (%FS) was also significantly decreased (23.52 ± 2.57 %) compared to Non-Tg (37.03 ± 2.97 %). The decreased %EF and %FS was not accompanied by a decreased cardiac output (CO) due to an elevated EDV at both time points. Of note, alterations in all the parameters described above were detected as early as two months of age.

Pressure volume loops (PV loops) were employed to determine if the mutation altered baseline function and contractile reserve (Figure 4, Table 2) at 3 months. PV recordings showed that left ventricular contractile function was significantly decreased in the presence of the mutation with no effect on relaxation for both male and female D230N mice (Table 2). The slope of the end systolic pressure-volume relationship (ESPVR) and dP_{max} were also significantly decreased for D230N mice, consistent with decreased contractile performance (Figure 4, Table 2). Additionally, increases in ESV and EDV for were evident for D230N mice (Table 2). These PV recordings indicate a loss of contractile reserve for D230N mice and confirmed the extent of the systolic dysfunction observed via echocardiography.

Effect of the D230N Mutation on Myocellular Ca^{2+} Kinetics and Mechanics

To determine the effects of the mutation on Ca^{2+} homeostasis, myocytes were isolated from 4 to 6-month-old male D230N mice and their Non-Tg siblings. Mechanical function and intracellular Ca^{2+} transients were measured in myocytes at baseline and with β-adrenergic stimulation (isoproterenol). The rates of contraction and relaxation in D230N-Tm myocytes were significantly increased compared to Non-Tg (Figure 5A–C). Peak amplitude Ca^{2+} transients were significantly increased in D230N-Tm myocytes compared to Non-Tg at baseline (Figure 5D). Additionally, the rates of Ca^{2+} rise and fall were greater in D230N-Tm myocytes than Non-Tg at baseline (Figure 5D–F). The baseline sarcomere length of D230N-Tm myocytes was not significantly different than that of Non-Tg (Figure 5G). To determine whether the mutation alters the response to β-adrenergic stimulation, we measured the effect of isoproterenol on all parameters. An increase in the rate of contraction and relaxation was observed as well as increased rate of Ca^{2+} transients for both Non-Tg and D230N-Tm myocytes compared to their baseline values (Figure 5). The increase was less pronounced in D230N-Tm myocytes where the baseline is high compared to Non-Tg (Figure 5).

Effect of the D230N Mutation on Myofilament Activation

Regulated-*in vitro* motility (R-IVM) was employed to study the effect of the D230N mutation on Tm regulation of myofilament activation (Figure 6, Table 3). Maximum sliding velocity (V_{max}) of filaments carrying the D230N-Tm was lower than that of WT-Tm filaments with values of 5.055 ± 0.060 μm/sec and 5.208 ± 0.029 μm/sec, respectively. The presence of D230N-Tm decreased the cooperativity of activation (n_H, Hill coefficient) as compared to WT-Tm with values of 1.04 ± 0.03 and 1.96 ± 0.05, respectively. The presence of the D230N-Tm decreases the Ca^{2+} sensitivity (6.637 ± 0.012) compared to WT-Tm filaments (6.920 ± 0.007). This right shift in Ca^{2+} sensitivity supports observations from in-solution assays for this mutation that described a decrease in Ca^{2+} sensitivity of ATPase activity in filaments carrying the D230N mutation [3]. Additionally, a greater percentage of WT-Tm filaments are moving uniformly compared to D230N-Tm filaments (Figure 6B).

Thermal Stability and Structure of D230N Tm

To study the effects of the mutation on the secondary structure and thermal stability of WT and D230N-Tm circular dichroism (CD) was employed. It has been previously shown that the secondary structure of Tm is nearly 100% alpha helical [38]. CD spectra of WT-Tm and D230N-Tm confirmed nearly 100% alpha helical structure with no statistical difference between them (Figure 7 inset). The thermal stability of D230N-Tm was also measured via

CD and compared to WT-Tm. The mean residual elipticity at 222 nm was plotted as a function of temperature to determine their thermal transitions or melt temperatures (T_m) (Figure 7, Table 4). The T_m for WT-Tm (44.2 ± 0.1) vs D230N-Tm (45.4 ± 0.1) was significantly different, suggesting that the D230N mutation increases the thermal stability of Tm consistent with a decreased flexibility for D230N-Tm compared to WT-Tm.

To further evaluate the stability of WT and mutant Tm the thermal stability was measured via differential scanning calorimetry (DSC). An advantage of this technique is that it allows separate characterization of the two calorimetric domains, or thermal transitions, of Tm unfolding that correspond to the N- and C-terminus, thus providing regional data on the effect of the mutation [12, 39, 40]. D230N-Tm exhibited significantly increased thermal stability as compared to WT-Tm, for the Cterminus, (D230N-Tm domain-1 (d1) 44.7 ± 0.06 °C, domain-2 (d2) 52.8 ± 0.10 °C; WT-Tm d1 43.7 ± 0.06 °C, d2 53.1 ± 0.10 °C) as can be seen by a rightward shift in the peak T_m values for the mutant (Figure 7, Table 4). This shift is significantly more pronounced in the first domain (d1) corresponding to the C-terminus of Tm indicating that the C-terminus (proximal to the mutation) is less flexible for D230N-Tm than WT-Tm. The shift in T_m for d1 was accompanied by a significant increase in the Van't Hoft enthalpy (ΔH_{VH}) of approximately 20% from WT-Tm (D230N-Tm d1 693 ± 8 kJ/mol (69% total), d2 448 ± 21 kJ/mol (31% total); WT-Tm d1 604 ± 19 kJ/mol (56% total), d2 381 ± 9 kJ/mol (44% total)) (Table 4). This increase in T_m (directly related to the free energy) is a result of an increase in ΔH_{VH}.

Of note, the N-terminus (d2) was also affected by the mutation despite being much further from residue 230 indicating that the mutation's effects can be propagated a significant distance (Figure 7, Table 4). A statistically significant decrease in ΔH_{VH} from WT to D230N Tm, and a small decrease in T_m was also observed.

Discussion

While the genetic basis of HCM and DCM is widely recognized, our understanding of the precise mechanisms that lead to pathogenic ventricular remodeling is incomplete. Therefore, the development of animal models with strong phenocopies and interrogation across multiple levels of biological complexity is central to identifying novel and effective therapeutics. The D230N mutation in Tm was first linked to DCM in a comprehensive study of two large multi-generational families [3]. To determine how a single point amino acid mutation in Tm gave rise to such a severe, highly penetrant DCM we generated a novel murine model expressing the D230N mutation. This murine model allowed us to track disease progression and ventricular remodeling over time as well as identify cellular mechanisms that could lead to disease. Gross morphological (Figure 2) and functional measurements (Figure 4, Tables 1 and 2) revealed severe systolic dysfunction with reduced cardiac contractility and increased end systolic volume in the absence of inflammatory changes or fibrosis (Figure 3). These changes, evident as early as 2 months of age, are indicative of a primary DCM with loss of contractile reserve and recapitulate the unique early onset human phenotype. Of note, PV loop recordings also indicated a sex-dependent difference between male and female animals carrying the D230N mutation that merits further investigation. In agreement with previous studies, our regulated *in vitro* motility

results revealed decreased Ca^{2+} sensitivity of sliding velocity coupled with a decreased cooperativity of activation (Figure 6) [3, 41]. Decreased Ca^{2+} sensitivity is a commonly reported finding in models of DCM but may not be sufficient to explain the complex pathology observed in the current model [5].

Further investigation of the Ca^{2+} handling and cellular mechanics in isolated myocytes showed an increase in Ca^{2+} transients including peak amplitude consistent with the observed increased rate of contraction and relaxation (Figure 5). The unidirectional change of these parameters indicates functional excitation-contraction coupling in D230N-Tm myocytes consistent with a compensatory response to a primary decrease in Ca^{2+} sensitivity [42]. D230N-Tm myofilaments may require more Ca^{2+} to generate the same response as WT myofilaments. Increased peak Ca^{2+} amplitudes suggest an increase in cytosolic Ca^{2+} whose availability would lead to activation of more myofilaments. As a result, more cross-bridges would form, thus compensating for the Ca^{2+} desensitization and allowing for sufficient force generation during contraction. These data are consistent with the findings in a previous knock-in mouse model of DCM caused by the ΔK210 mutation in cTnT where the Ca^{2+} transients in isolated myocytes were also increased compared to Non-Tg myocytes [43]. Of note, isoproterenol stimulated D230N-Tm cells had a significantly lower percent increase in Ca^{2+} transients from baseline compared to Non-Tg cells (Figure 5H). This diminished capacity to respond to beta-adrenergic stimulation, in D230N myocytes, is likely due to the nearly 2 fold increase in field stimulated Ca^{2+} release at baseline compared to Non-Tg.

While our mouse model accurately phenocopied the human disease, the primary mechanistic link between genotype and phenotype remained unclear. Thus, we sought to determine the structural effects of the D230N mutation. The alpha-helical coiled-coil structure of Tm is essential for its function [44]. The head-to-tail overlap arrangement of sequential Tm dimers in the sarcomere is required for the cooperativity of myofilament activation [44]. Therefore, it is not surprising that a mutation causing an alteration in tertiary structure could affect the ability of Tm to form coiled-coils, polymerize, or interact with other thin filament proteins at a distance. Previous studies had demonstrated that a Tm variant (D137L) caused small local changes in flexibility that propagate much larger effects to a site 38 amino acids away [13–15]. More recently it was shown that D137L altered the flexibility of Tm leading to changes in the regulatory function of the protein [12]. Additionally, Hodges et al. showed that single point amino acid substitutions in Tm can propagate destabilization along the coiled coil as far as 165Å away [45]. CD studies revealed no change in overall alpha helicity of D230N-Tm versus WT, which was not surprising as large changes in Tm helicity would significantly impact viability. The overall thermal stability of the WT-Tm versus D230N-Tm, however, was significantly increased indicating that the flexibility of filaments containing D230N-Tm is decreased resulting in a more rigid Tm. These data could indicate propagating structural effects to the termini of Tm that alter the stability of the crucial overlap region thus altering the regulatory function of Tm (Figure 7, Table 4).

To further expand our D230N-Tm thermal stability results to include regional data on the structural effects of the mutation, we utilized DSC. The power of this technique in the context of Tm is the ability to inform on the thermal stability of both the N- and C-terminal regions of the molecule and thus determine if the mutational effects propagate to the ends of

Tm. It should be noted that the use of the term “flexibility” to describe changes in the thermal stability of Tm has been well established in previous publications [12, 46–49]. We found that the overall thermal stability of Tm was increased for D230N-Tm and strikingly this increase was more profound at the C-terminus proximal to the mutation (Figure 7, Table 4). This suggests that the C-terminus is less flexible, or more rigid, in the presence of D230N-Tm. We also observed, (at a significant distance), that the N-terminus of D230N-Tm exhibited a significantly decreased enthalpy (ΔH_{VH}) with no change in thermal stability (T_m). This could suggest enthalpy-entropy compensation where more favorable entropy causes the solvation shells around D230N-Tm to loosen at the N-terminus of the molecule destabilizing it and further altering the flexibility of Tm and therefore its regulatory function. These changes, at each terminus, lend support to our hypothesis that D230N-Tm causes propagating structural effects that can alter thin filament regulatory function.

Importantly, our finding of decreased Tm flexibility for this DCM causing mutation is the opposite of what was reported for HCM causing mutations, suggesting an intrinsic relationship between the flexibility of Tm and phenotypic cardiac pathology [50–52]. Of note, it was recently shown that HCM-linked mutations in the Tn-binding site of Tm (I172T, L185R, and E180V) cause differential effects on the thermal stability of Tm despite being phenotypically similar [53]. This further demonstrates our incomplete understanding of how single amino acid mutations lead to a complex series of cardiomyopathies and underscores our need for accurate animal models and eventually specific therapies. It is likely that mutations in the regulatory Tm that alter its thermal stability and flexibility lead to disease in a specific manner dependent on the precise amino acid change and location (periodically and helically) on Tm.

Our results suggest that for D230N-Tm the induced structural changes could hinder the azimuthal shift of Tm along actin from the blocked (B) to closed (C) state, via decreased flexibility, thus impairing the initiation of muscle activation. As Ca^{2+} levels rise and bind to cTnC, D230N-Tm’s rigidity could hinder its movement, thus masking myosin binding sites on actin, resulting in the observed decrease in Ca^{2+} sensitivity of sliding velocity and cooperativity of activation (Figure 6A, Table 3). A concomitant increase in peak Ca^{2+} amplitude, a likely compensatory response to this altered B→C equilibrium, then occurs in an attempt to force the transition from B→C state and maintain the hearts force generating capacity (Figure 5D–F). Indeed, this hypothesis is in agreement with studies that suggest that for a semi-flexible Tm a change in innate flexibility could result in altered Ca^{2+} sensitivity and change the number of available myosin binding sites [54]. The C to open (O) transition then occurs rapidly as myosin binds and pushes the more rigid Tm out of the groove. This rapid transition is evidenced by an increase in the baseline rate of contraction for D230N-Tm myocytes (Figure 5B). Additionally, a decrease in the percent uniformly motile filaments containing D230N-Tm at activating calcium supports a disrupted equilibrium (Figure 6B). The parallel increase in erratic movement, defined as a standard deviation > 50% of the mean filament speed, could be conferred by the increased rigidity of D230N-Tm [30]. Together, these changes could lead to a biased activation equilibrium, in which the closed position becomes an activation barrier, causing downstream signaling that eventually results in the observed pathology. The precise link(s) between impaired activation and complex cardiac remodeling require further study including the identification of the

earliest differential signaling cascades that would determine the natural history of the remodeling that defines dilated cardiomyopathic remodeling *in vivo*.

In summary, we've generated an accurate, highly progressive model of genetic DCM that advances our understanding of how a single amino acid mutation can lead to a severe primary disease of the heart muscle. This model provides a critical link that demonstrates how structural changes in the regulatory thin filament that effect its flexibility can ultimately effect pathology at the whole heart level. Further study into the precise structural changes undergone by Tm, and its interaction with subsequent Tm dimers at the overlap in the presence of the mutation will be an important future direction. It's possible that the effects of the mutation propagate through the Tm overlap, decreasing the flexibility of the Tm filament along its length. Advancing our understanding of this structure-function relationship could lead to disease-modifying therapies at the level of the sarcomere to treat the earliest stages and alter the natural history of this disorder.

Supplementary Material

Refer to Web version on PubMed Central for supplementary material.

Acknowledgments

Funding Sources

This work was supported by grants from the American Heart Association 16PRE27260116 and Heart, Lung, and Blood Training Grant T32-HL07249 to ML Lynn. Additional funding sources include NIH HL107046 and HL075619 and the Steven M. Gootter Foundation to JC Tardiff.

We would like to thank Dr. Colette Quinn for her assistance with DSC analysis and Dr. Chad Park for his help with CD analysis.

References

1. Geisterfer-Lowrance A, Kass S, Tanigawa G, Vosberg H, McKenna W, Seidman C, et al. A molecular basis for familial hypertrophic cardiomyopathy: a beta cardiac myosin heavy chain gene missense mutation. Cell. 1990; 62:999–1006. [PubMed: 1975517]
2. Force T, Bonow R, Houser S, Solaro R, Hershberger R, Adhikari B, et al. Research priorities in hypertrophic cardiomyopathy: Report of a working group of the national heart, lung, and blood institute. Circulation. 2010; 122:1130–3. [PubMed: 20837938]
3. Lakdawala N, Dellefave L, Redwood C, Sparks E, Cirino A, Depalma S, et al. Familial dilated cardiomyopathy caused by an alpha-tropomyosin mutation: The distinctive natural history of sarcomeric dilated cardiomyopathy. J Am Coll Cardiol. 2010; 55:320–9. [PubMed: 20117437]
4. Williams MR, Lehman SJ, Tardiff JC, Schwartz SD. Atomic resolution probe for allostery in the regulatory thin filament. Proceedings of the National Academy of Sciences of the United States of America. 2016; 113:3257–62. [PubMed: 26957598]
5. Robinson P, Griffiths PJ, Watkins H, Redwood CS. Dilated and Hypertrophic Cardiomyopathy Mutations in Troponin and α-Tropomyosin Have Opposing Effects on the Calcium Affinity of Cardiac Thin Filaments. Circulation Research. 2007; 101:1266–73. [PubMed: 17932326]
6. Gordon A, Regnier M, Homsher E. Skeletal and cardiac muscle contraction activation: Tropomyosin "rocks and rolls". News Physiol Sci. 2001; 16:49–55. [PubMed: 11390948]
7. Boussouf S, Geeves M. Tropomyosin and troponin cooperativity on the thin filament. Adv Exp Med Biol. 2007; 592:99–109. [PubMed: 17278359]

8. McKillop D, Geeves M. Regulation of the interaction between actin and myosin subfragment 1: Evidence for three states of the thin filament. Biophysical Journal. 1993; 65:693–701. [PubMed: 8218897]
9. Palm T, Graboski S, Hitchcock-DeGregori S, Greenfield N. Disease-causing mutations in cardiac troponin T: Identification of a critical tropomyosin-binding region. Biophys J. 2001; 81:2827–37. [PubMed: 11606294]
10. Nitanai Y, Minakata S, Maeda K, Oda N, Maeda Y. Crystal structures of tropomyosin: flexible coiled-coil. Adv Exp Med Biol. 2007; 592:137–51. [PubMed: 17278362]
11. Holmes K, Lehman W. Gestalt-binding of tropomyosin to actin filaments. J Muscle Res Cell Motil. 2008; 29:213–9. [PubMed: 19116763]
12. Yar S, Chowdhury S, Davis R, Kobayashi M, Monasky M, Rajan S, et al. Conserved Asp-137 is important for both structure and regulatory functions of cardiac α-tropomyosin (α-TM) in a novel transgenic mouse model expressing α-TM-D137L. J Biol Chem. 2013; 288:16235–46. [PubMed: 23609439]
13. Guinto P, Manning E, Schwartz S, Tardiff J. Computational characterization of mutations in cardiac troponin t known to cause familial hypertrophic cardiomyopathy. J Theor Comput Chem. 2007; 6:413–9. [PubMed: 26500385]
14. Nirody J, Li X, Sousa D, Sumida J, Fischer S, Leher S, et al. Electron microscopy and molecular dynamics on a D137L mutant of tropomyosin. 2010
15. Tardiff J. Thin filament mutations: Developing an integrative approach to a complex disorder. Circ Research. 2011; 108:765–82.
16. Tardiff J, Factor S, Tompkins B, Hewett T, Palmer B, Moore R, et al. A truncated cardiac troponin t molecule in transgenic mice suggests multiple cellular mechanisms for familiar hypertrophic cardiomyopathy. J Clin Invest. 1998; 101:2800–11. [PubMed: 9637714]
17. Tardiff J, Hewett T, Palmer B, Olsson C, Factor S, Moore R, et al. Cardiac troponin t mutations result in allele specitic phenotypes in a mouse model for hypertrophic cardiomyopathy. J Clin Invest. 1999; 104:469–81. [PubMed: 10449439]
18. Rajan S, Ahmed R, Jagatheesan G, Petrachevskaya N, Boivin G, Urboniene D, et al. Dilated cardiomyopathy mutant tropomyosin mice develop cardiac dysfunction with significantly decreased fractional shortening and myofilament calcium sensitivity. Circ Research. 2007; 101:205–14.
19. Guinto P, Haim T, Dowell-Martino C, Sibinga N, Tardiff J. temporal and mutation-specific alterations in ca2+ homeostasis differentially determine the progression of ctnt-related cardiomyopathies in murine models. Am J Physiol Heart Circ Physiol. 2009; 297:H614–26. [PubMed: 19502551]
20. Schneider CA, Rasband WS, Eliceiri KW. NIH Image to ImageJ: 25 years of image analysis. Nature methods. 2012; 9:671–5. [PubMed: 22930834]
21. Rice R, Guinto P, Dowell-Martino C, He H, Hoyer K, Krenz M, et al. Cardiac myosin heavy chain isoform exchange alters the phenotype of cTnT-related cardiomyopathies in mouse hearts. J Mol Cell Cardiol. 2010; 48:979–88. [PubMed: 20004663]
22. Methawasin M, Strom JG, Slater RE, Fernandez V, Saripalli C, Granzier H. Experimentally Increasing the Compliance of Titin Through RNA Binding Motif-20 (RBM20) Inhibition Improves Diastolic Function In a Mouse Model of Heart Failure With Preserved Ejection Fraction. Circulation. 2016; 134:1085–99. [PubMed: 27630136]
23. Haim T, Dowell-Martino C, Diamanti T, Scheuer J, Tardiff J. Independent fhc-related cardiac troponin t mutations exhibit specific alterations in myocellular contractility and calcium kinetics. J Mol Cell Cardiol. 2007; 42:1098–110. [PubMed: 17490679]
24. Hitchcock-DeGregori S, Heald R. Altered actin and troponin binding of amino-terminal variants of chicken striated muscle alpha-tropomyosin expressed in escherichia coli. J Biol Chem. 1987; 262:9730–35. [PubMed: 2954961]
25. Monteiro P, Lataro R, Ferrom JR, F C. Functional alpha-tropomyosin produced in escherichia coli. A dipeptide extension can substitute the amino-terminal acetyl group. J Biol Chem. 1994; 269:10461–66. [PubMed: 8144630]

26. Sumandea M, Pyle W, Kobayashi T, de Tombe P, Solaro R. Identification of a functionally critical protein kinase c phosphorylation residue of cardiac troponin t. J Biol Chem. 2003; 278:35135–144. [PubMed: 12832403]
27. Manning EP, Guinto PJ, Tardiff JC. Correlation of Molecular and Functional Effects of Mutations in Cardiac Troponin T Linked to Familial Hypertrophic Cardiomyopathy: AN INTEGRATIVE IN SILICO/IN VITRO APPROACH. The Journal of Biological Chemistry. 2012; 287:14515–23. [PubMed: 22334656]
28. Margossian S, Lowey S. Preparation of myosin and its subfragments from rabbit skeletal muscle. Methods in Ezymology. 1982; 85:55–71.
29. Kron S, Toyoshima Y, Uyeda T, Spudich J. Assays for actin sliding movement over myosin-coated surfaces. Methods in Ezymology. 1991; 196:399–416.
30. Homsher E, Kim B, Bobkova A, Tobacman L. Calcium regulation of thin filament movement in an in vitro motility assay. Biophys J. 1996; 70:1881–92. [PubMed: 8785348]
31. Homsher E, Lee D, Morris C, Pavlov D, Tobacman L. Regulation of force and unloaded sliding speed in single thin filaments: Effects of regulatory proteins and calcium. J Physiol. 2000; 524(Pt 1):233–43. [PubMed: 10747195]
32. Homsher E, Nili M, Chen I, Tobacman L. Regulatory proteins alter nucleotide binding to acto-myosin of sliding filaments in motility assays. Biophys J. 2003; 85:1046–52. [PubMed: 12885651]
33. Homsher E, Wang F, Sellers J. Factors affecting movement of f-actin filaments propelled by skeletal muscle heavy meromyosin. Am J Physiol. 1992; 262:C714–23. [PubMed: 1550212]
34. Greenfield N. Using circular dichroism collected as a function of temperature to determine the thermodynamics of protein unfolding and binding interactions. Nat Protoc. 2006; 1:2527–35. [PubMed: 17406506]
35. Pankuweit S, Richter A, Ruppert V, Maisch B. Classification of cardiomyopathies and indication for endomyocardial biopsy revisited. Herz. 2009; 34:55–62. [PubMed: 19214409]
36. Maisch B, Noutsias M, Ruppert V, Richter A, Pankuweit S. Cardiomyopathies: Classification, diagnosis, and treatment. Heart Fail Clin. 2012; 8:53–78. [PubMed: 22108727]
37. Perriard J, Hirschy A, Ehler E. Dilated cardiomyopathy: A disease of the intercalated disc? Trends Cardiovasc Med. 2003; 13:30–8. [PubMed: 12554098]
38. Phillips G Jr, Fillers J, Cohen C. Tropomyosin crystal structure and muscle regulation. J Mol Biol. 1986; 192:111–31. [PubMed: 3820299]
39. Kremneva E, Nikolaeva O, Gusev N, Levitsky D. Effects of troponin on thermal unfolding of actin bound tropomyosin. Biochemistry. 2003; 68:976–84. [PubMed: 14606939]
40. Matyushenko A, Artemova N, Sluchanko N, Levitsky D. effects of two stabilizing mutations, D137L and G126R, in the middle part of α-tropomyosin on the domain structure of its molecule. Biophys Chem. 2015; 196:77–85. [PubMed: 25451681]
41. Mirza M, Marston S, Willott R, Ashley C, Mogensen J, McKenna W, et al. Dilated cardiomyopathy mutations in three thin filament regulatory proteins result in a common functional phenotype. J Biol Chem. 2005; 280:28498–506. [PubMed: 15923195]
42. Schober T, Huke S, Venkataraman R, Gryshchenko O, Kryshtal D, Hwang H, et al. Myofilament ca sensitization increases cytosolic ca binding affinity, alters intracellular ca homeostasis, and causes pause-dependent ca-triggered arrhythmia. Circulation Research. 2012; 111:170–9. [PubMed: 22647877]
43. Du C, Morimoto S, Nishii K, Minakami R, Ohta M, Tadano N, et al. Knock-in mouse model of dilated cardiomyopathy caused by troponin mutation. Circ Research. 2007; 101:185–94.
44. Greenfield N, Hitchcock-DeGregori S. the stability of tropomyosin, a two stranded coiled-coil protein, is primarily a function of the hydrophobicity of residues at the helix-helix interface. 1995
45. Kirwan J, Hodges R. Transmission of Stability Information through the N-domain of Tropomyosin Is Interupted by a Stabilizing Mutation (A109L) in the Hydrophobic Core of the Stability Control Region (Residues 97–118). J Biol Chem. 2013; 289:4356–66. [PubMed: 24362038]
46. Singh A, Hitchcock-DeGregori S. Local destabalization of the tropomyosin coiled coil gives the molecular flexibility required for actin binding. Biochemistry. 2003; 42:14114–21. [PubMed: 14640678]

47. Singh A, Hitchcock-DeGregori S. Dual requirement for flexibility and specificity for bidning of the coiled-coil tropomyosin to its target, actin. Structure. 2006; 14:43–50. [PubMed: 16407064]

48. Sumida J, Wu E, Leher S. Conserved Asp-137 imparts flexibility to tropomyosin and affects function. J Biol Chem. 2007; 283:6728–34. [PubMed: 18165684]

49. Nevzorov I, Nikolaeva O, Kainov Y, Redwood C, Levitsky D. Conserved noncanonical residue gly-126 confers instability to the middle part of the tropomyosin molecule. J Biol Chem. 2011; 286:15766–72. [PubMed: 21454502]

50. Heller M, Nili M, Homsher E, Tobacman L. Cardiomyopathic tropomyosin mutations that increase thin filament Ca2+ sensitivty and tropomyosin N-domain flexibility. J Biol Chem. 2003; 278:41742–8. [PubMed: 12900417]

51. Kremneva E, Boussouf S, Nikolaeva O, Maytum R, Geeves M, Levitsky D. Effects of two familial hypertrophic cardiomyopathy mutations in alpha tropomyosin, Asp175Asn and Glu180Gly, on the thermal unfolding of actin-bound tropomyosin. Biophys J. 2004; 87:3922–33. [PubMed: 15454401]

52. Loong CKP, Zhou H-X, Chase PB. Familial hypertrophic cardiomyopathy related E180G mutation increases flexibility of human cardiac α- tropomyosin. FEBS Letters. 2012; 586:3503–7. [PubMed: 22958892]

53. Matyushenko AM, Shchepkin DV, Kopylova GV, Popruga KE, Artemova NV, Pivovarova AV, et al. Structural and Functional Effects of Cardiomyopathy-Causing Mutations in the Troponin T-Binding Region of Cardiac Tropomyosin. Biochemistry. 2017; 56:250–9. [PubMed: 27983818]

54. Loong CKP, Badr MA, Chase PB. Tropomyosin Flexural Rigidity and Single Ca(2+) Regulatory Unit Dynamics: Implications for Cooperative Regulation of Cardiac Muscle Contraction and Cardiomyocyte Hypertrophy. Frontiers in Physiology. 2012; 3:80. [PubMed: 22493584]

Research Highlights

- We generated a novel, accurate, and highly progressive mouse model of genetic DCM.
- Altered tropomyosin stability was identified as mechanistic for DCM.
- There is a link between tropomyosin overlap flexibility and cardiac function.

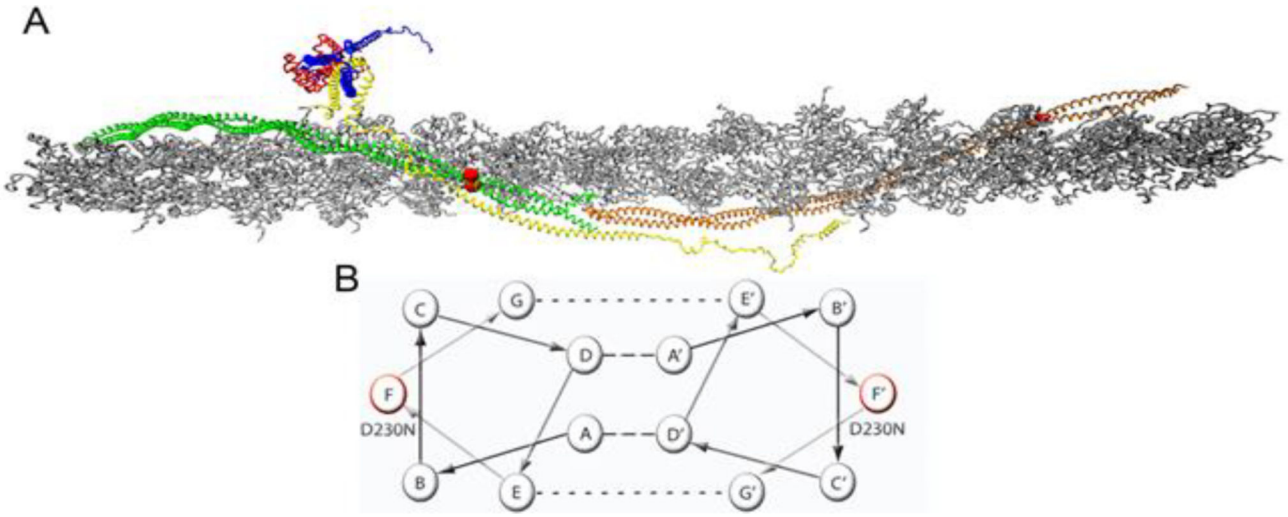

Figure 1.

Atomistic Model of the Cardiac Thin Filament. (A) Average structure taken over 10 ns in a molecular dynamic simulation, (Williams et al. 2016). Grey – filamentous actin (F-actin), Green/Orange – adjacent Tm dimers, Yellow – cardiac Troponin T (cTnT), Red – cardiac Troponin C (cTnC), Blue – cardiac Troponin I (cTnI). Red balls indicate the position of the D230N-Tm mutation. (B) Representative helical wheel of two interacting Tm monomers, monomer one contains a seven heptad repeat (positions A–G) and monomer 2 contains the same repeat (positions A'–G'). Residues in positions A and D are typically hydrophobic (dashed line) and stabilize the core of the dimer. Residues in positions E and G typically salt bridges (dotted line) to further stabilize the dimer. Residues B, C, and F are solvent exposed and can interact with neighboring proteins. The helical position of D230N is marked in red on both monomers.

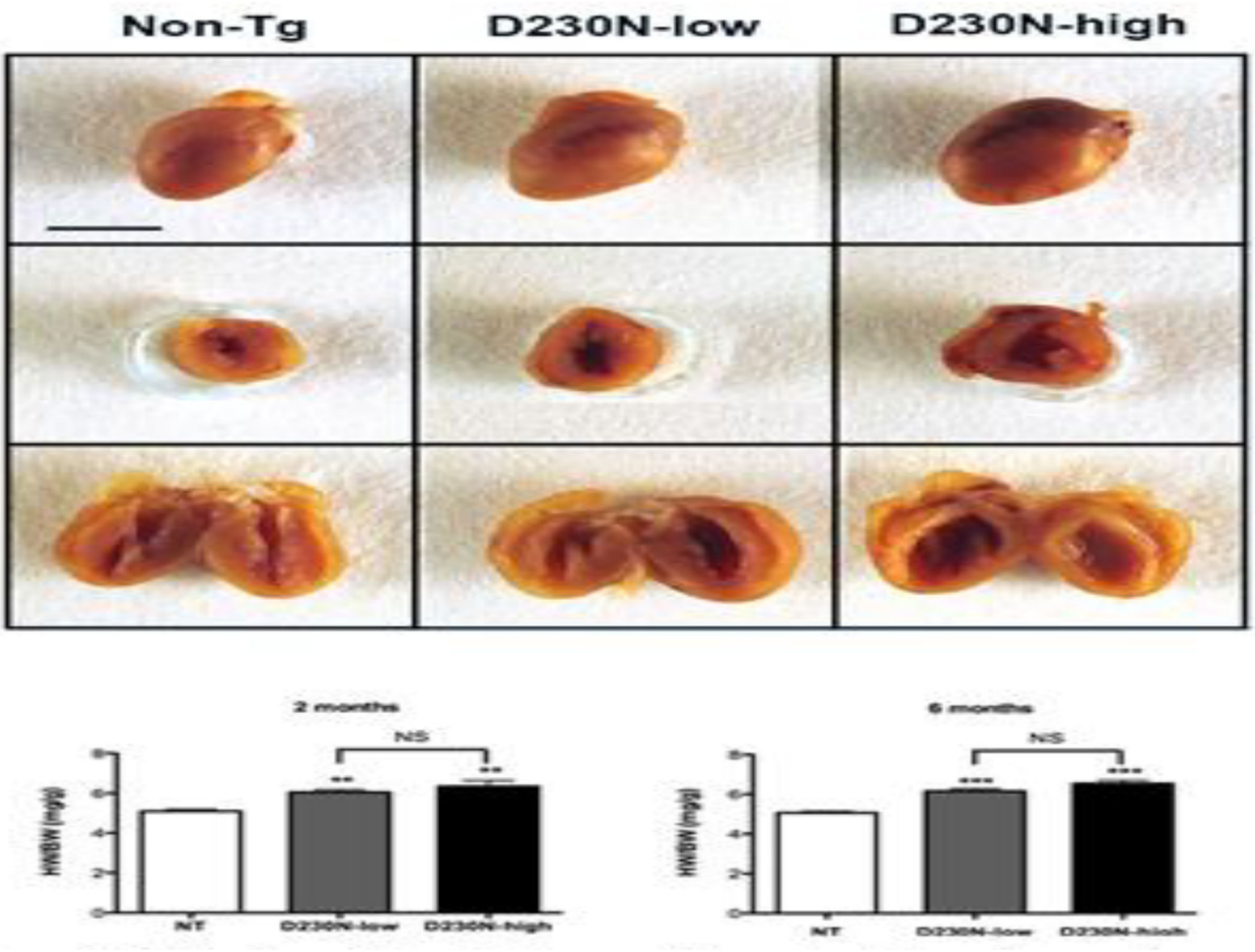

Figure 2.

Cardiac Morphology of hearts taken from 6 month old Non-Tg (NT), D230N-low, and D230N-high hearts. (A) Top - whole hearts, Middle - transverse section, Bottom - sagittal section. Line represents 5 mm. (B–C) Heart weight/body weight (HW/BW) measurements of 2 and 6 month old, Non-tg, D230N-low, and D230N-high mice. Values are expressed as mean ± S.E.M. One-way ANOVA and Newman Keuls post hoc analysis was used for statistical comparison to Non-tg. * $p < 0.05$, ** $p < 0.01$, *** $p < 0.001$, NS not significant.

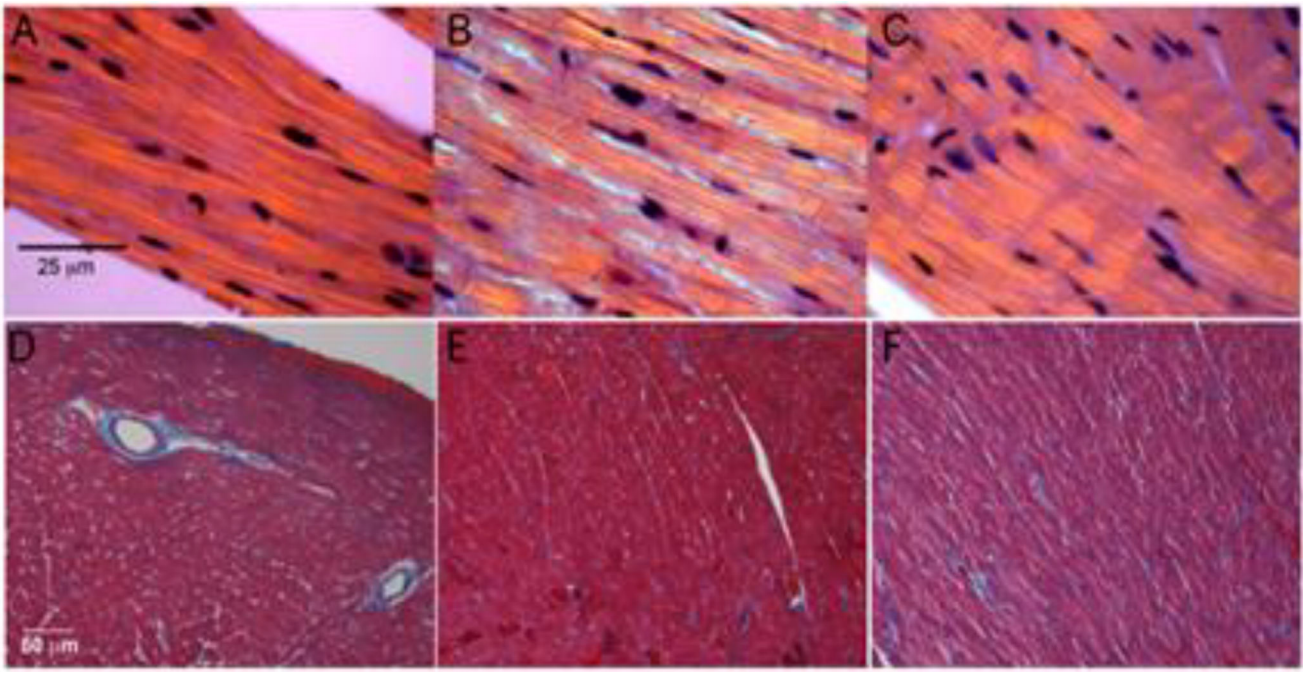

Figure 3.

Left Ventricular Histology. (A–C) Hematoxylin and eosin stain of cardiac left ventricular fibers under polarized light. (A) 6 month old Non-tg, (B) D230N-low, and (C) D230N-high mice. Line represents 25 μm. (D–F) Masson's trichrome stain of sections from cardiac left ventricles. (D) Non-tg, (E) D230N-low, and (F) D230N-high mice. Line represents 50 μm.

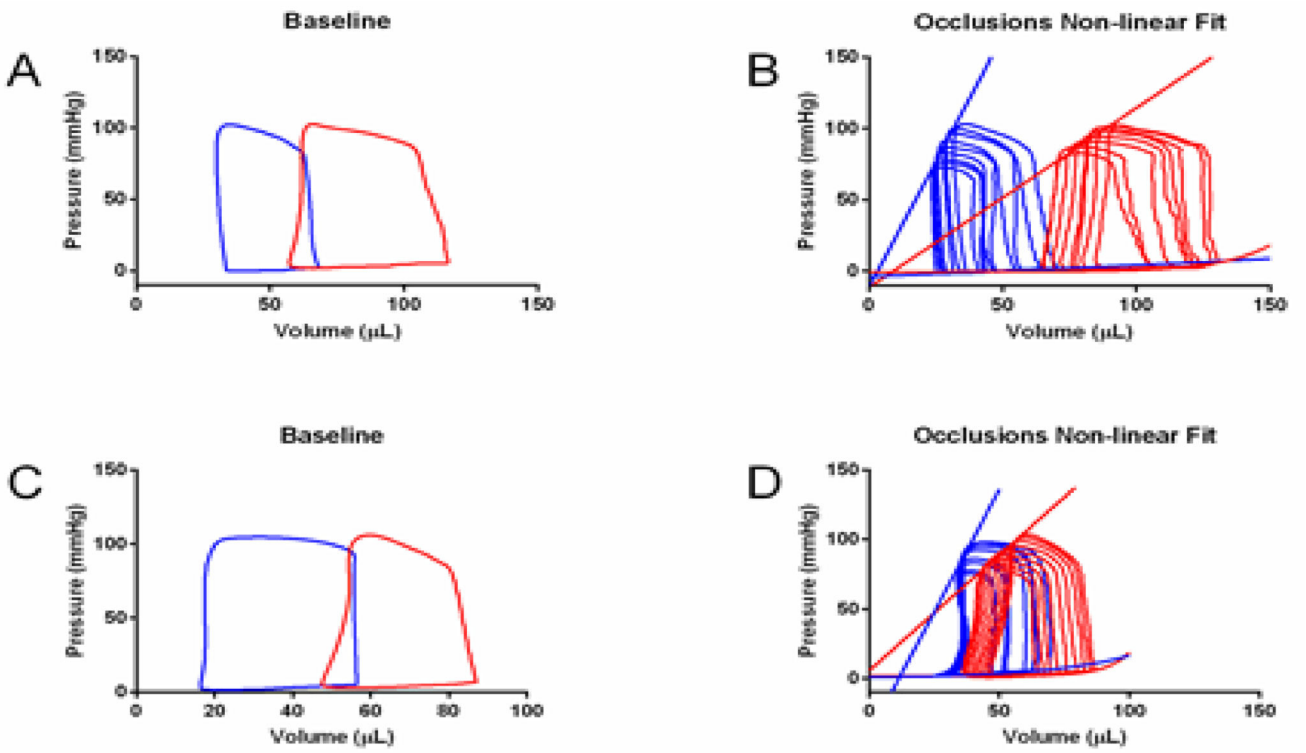

Figure 4.

Baseline and Occlusion Pressure-Volume Loops for Non-tg (Blue) and D230N-Tm (Red) mice. (A–B) male, (C–D) female aged 3 months. N = 3–4 per group. Values are summarized in Table 2.

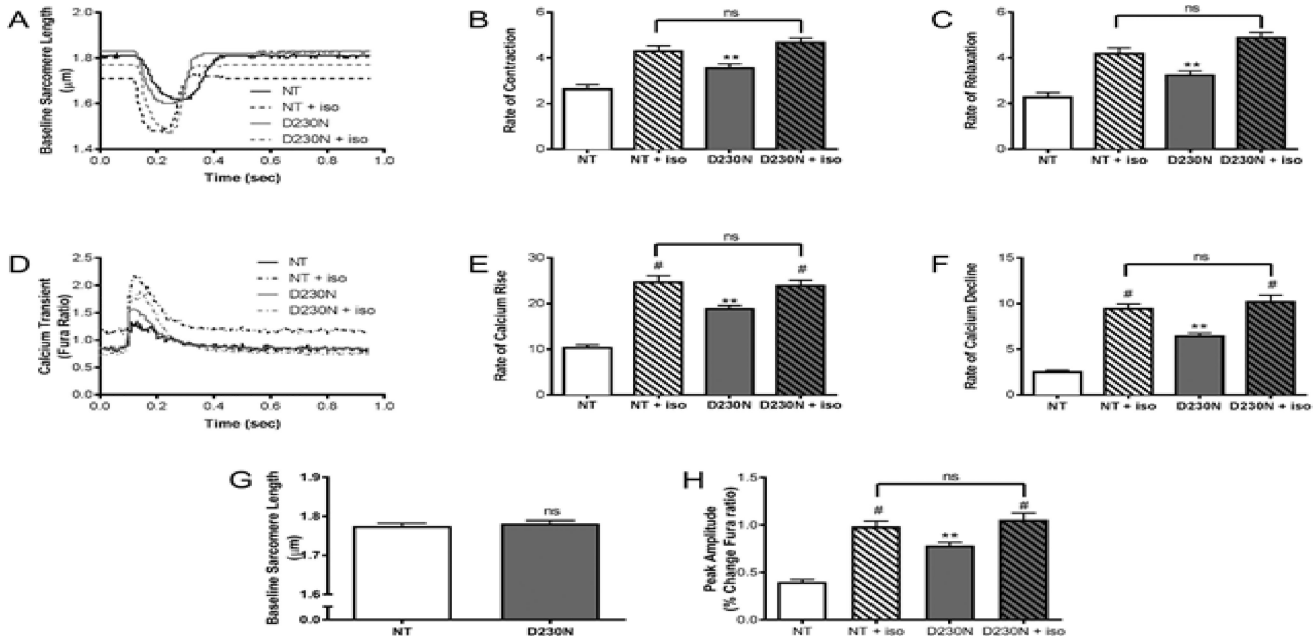

Figure 5.

Myocellular mechanics and Intracellular Calcium Transients from field stimulated ventricular myocytes (A) Representative contraction/relaxation recordings from 4–6 month old male Non-Tg and D230N-high transgenic myocytes. (B–C) Cardiac myocyte mechanical measurements. (D) Representative calcium transient recordings from 4–6 month old Non-Tg and D230N-high transgenic myocytes. (E–F) Cardiac myocyte calcium transient measurements. (G) Baseline sarcomere length and (H) peak calcium transient amplitude of D230N-Tm myocytes vs. WT-Tm myocytes. An n = 4–5 animals were used for each group with at least 30 cells analyzed. Values expressed as mean ± S.E.M. Two-way ANOVA was used for statistical analysis with a Bonferonni post test. ** $p < 0.01$ in comparison to NT, # $p < 0.05$ baseline versus isoproterenol (ISO).

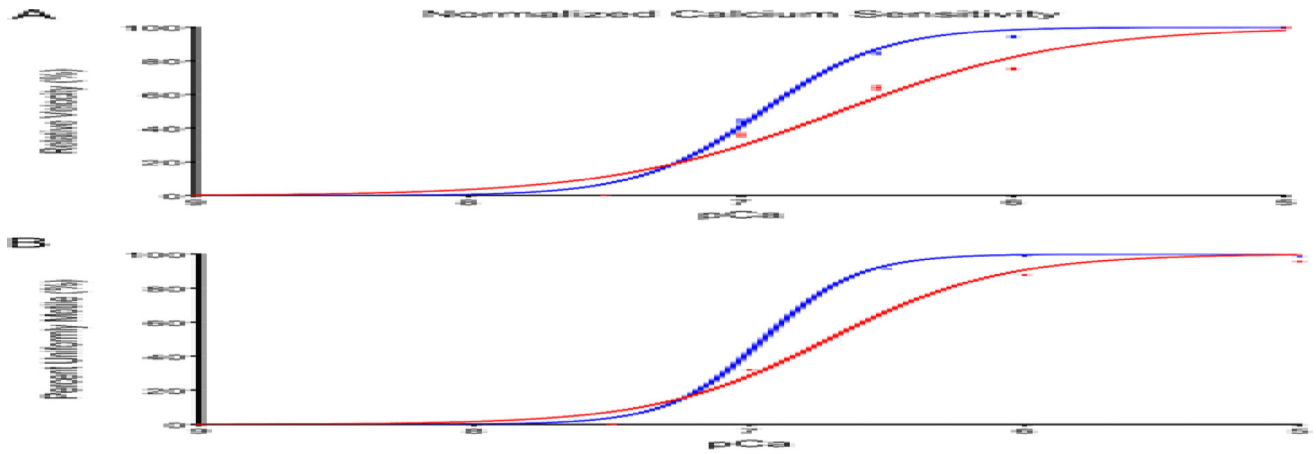

Figure 6.

Regulated-*In Vitro* Motility assays of filaments containing WT (blue) or D230N-Tm (red) at varying calcium concentrations showing the (top) normalized velocity of filament sliding as a function of pCa (bottom) percent uniformly motile filaments. V_{max} values are reported as means of the filament sliding velocity at pCa 5. The EC_{50} and slope values were obtained from normalized fits of the Hill equation to mean filament speed at each pCa; 150 filaments per condition were analyzed. Values are expressed as mean ± S.E.M and summarized in Table 3. A student's t test was used for statistical comparison. *** $p < 0.001$ relative to WT filaments.

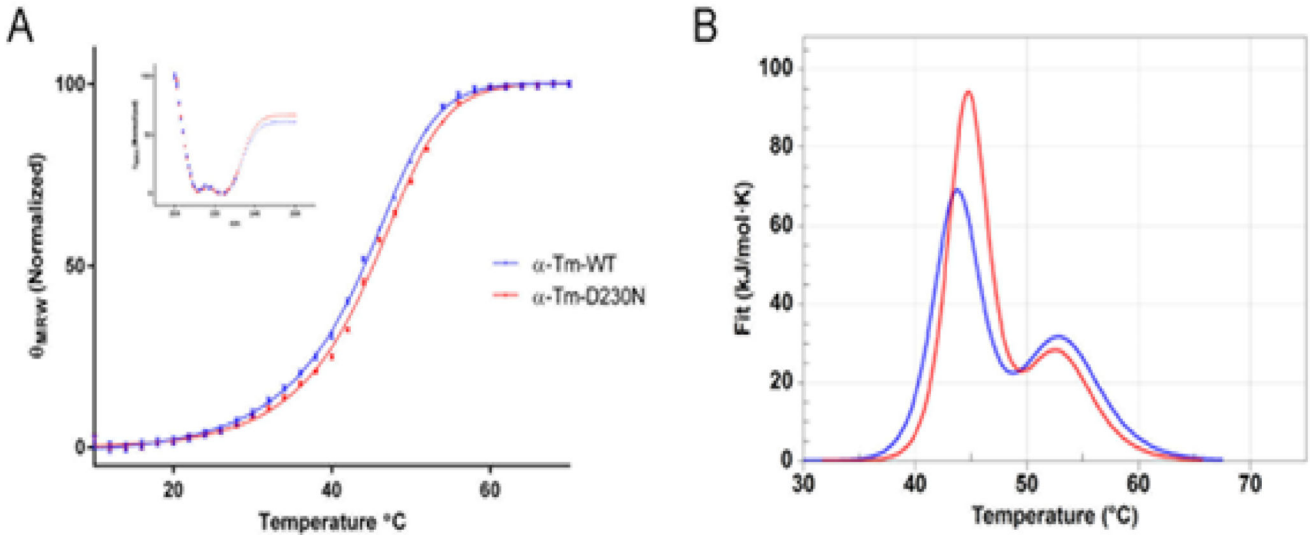

Figure 7.

Thermal Stability and Structure of human WT and D230N-Tm assessed via CD and DSC. (A) The mean residue elipticity of 0.3 mg/mL WT (blue) and D230N (red) at 222 nm is graphed as a function of temperature. Inset: Spectra from 200 to 260 nm of WT and D230N-Tm at 20°C. n=3, each an average of 3–5 scans. Extra sum of squares F test and least squares fit analysis were used for statistical comparison of WT to D230N-Tm. (B) Thermal Stability of WT and D230N-Tm assessed via DSC. The heat capacity (kJ/mol*K) of 1.8 mg/mL WT (blue) and D230N (red) Tm is graphed as a function of temperature. Solid lines represent experimental fit after subtraction of baseline and instrumental background. The heating rate was 1°C/min from 20–70°C. Reported values were determined from the fit of the two curves (Van't Hoff two-state model), one-way ANOVA was used to determine statistical significance. Values in Table 4 are reported as mean ± S.E.M **p < 0.01, ****p < 0.0001 compared to WT-Tm.

Table 1

Summary of Echocardiographic Parameters obtained at 2 and 6 months for mixed gender D230N-Tm hearts. Left ventricular internal diameter in diastole and systole ($LVID_d$ and $LVID_s$ respectively), end diastolic volume (EDV), end systolic volume (ESV), ejection fraction percent (%EF), fractional shortening percent (%FS), cardiac output (CO).

	2 Months		6 Months	
	Non-Tg	**D230N-Tm**	**Non-Tg**	**D230N-Tm**
$LVID_d$(mm)	3.74 ± 0.05	4.03 ± 0.06**	3.84 ± 0.89	4.38 ± 0.08**
$LVID_s$ (mm)	2.28 ± 0.08	2.96 ± 0.16**	2.51 ± 0.11	3.36 ± 0.17**
EDV (μl)	59.73 ± 1.76	71.41 ± 2.55**	64.73 ± 4.37	87.01 ± 3.89**
ESV (μl)	18.02 ± 1.58	34.30 ± 4.60**	23.49 ± 2.95	46.78 ± 6.02*
% EF	69.81 ± 2.41	51.83 ± 6.01**	67.11 ± 3.68	46.78 ± 4.42**
% FS	38.92 ± 1.97	26.51 ± 3.84**	37.03 ± 2.97	23.52 ± 2.57**
CO (ml/min)	15.33 ± 1.66	17.66 ± 3.1	15.52 ± 1.73	15.11 ± 0.97

Values are expressed as Mean ± S.E.M. Student's t-test was used for statistical comparison to Non-Tg

* $p \leq 0.05$,

** $p \leq 0.01$.

Table 2

Summary of Functional Parameters obtained from Baseline and Occlusion PV loops separated by gender at 3 months of age (Figure 4). Rate of pressure change maximum and minimum (dP_{max} and dP_{min}), end systolic volume (ESV), end diastolic volume (EDV), end systolic pressure volume relationship (ESPVR), end diastolic pressure volume relationship (EDPVR).

	Non-Tg (male)	D230N-Tm (male)	Non-Tg (female)	D230N-Tm (female)
dP_{max} (mmHg/sec)	9256.3 ± 806.9	6894.4 ± 501.2*	9273.7 ± 979.7	5900.4 ± 515.4#
dP_{min} (mmHg/sec)	−8830.74 ± 756.5	−8919.5 ± 681.4	−7806.0 ± 210.7	−7241.0 ± 876.4
ESV (uL)	27.1 ± 4.3	55.4 ± 7.3*	13.37 ± 3.3	45.1 ± 6.4#
EDV (uL)	65.8 ± 6.3	102.9 ± 12.2*	42.0 ± 7.9	78.7 ± 8.0#
ESPVR	3.8 ± 0.3	2.1 ± 0.3*	4.6 ± 0.03	1.9 ± 0.1####
EDPVR	0.03 ± 0.004	0.03 ± 0.01	0.04 ± 0.004	0.05 ± 0.01

Values are reported mean ± S.E.M. student's t test was used to assess significance vs Non-Tg.

* $p < 0.05$, compared to Non-Tg males,

# $p < 0.05$,

$p < 0.0001$ compared to Non-Tg females. N = 3–4.

Table 3

Summary of Velocity-pCa Relationship for *in vitro* motility data (Figure 6).

	V_{max}	EC_{50}	n_H
α-Tm-WT	5.208 ± 0.030	6.920 ± 0.007	1.956 ± 0.054
α-Tm-D230N	5.055 ± 0.060 ***	6.637 ± 0.012 ***	1.043 ± 0.028 ***

Values are reported as Mean ± S.E.M.

*** $p < 0.001$ compared to WT-Tm.

Table 4

Summary of Calorimetric Data obtained from DSC and melt temperature from CD (Figure 7) of WT-Tm and D230N-Tm.

	DSC				CD
	Domain-1 (C-terminus)		Domain-2 (N-terminus)		(Total Tm)
	T_m°C	ΔHkJ/mol (% total)	T_m°C	ΔHkJ/mol (% total)	T_m°C
α-Tm-WT	43.7 ± 0.06	604 ± 19 (56%)	53.1 ± 0.1	381 ± 9 (44%)	44.2 ± 0.1
α-Tm-D230N	44.7 ± 0.06 ****	693 ± 8 (69%)	52.8 ± 0.1 **	448 ± 21 (31%)	45.4 ± 0.1 ****

Values are reported as mean ± S.E.M.

** $p < 0.01$

**** $p < 0.0001$ compared to WT-Tm.